applied sciences

MDPI

Article

Design of Viscosity and Nozzle Path Using Food 3D Printer and Pneumatic Pressure Syringe-Type Dispensing System

Changuk Ji [1], Areum Cha [2] and Dongbin Shin [3,*]

[1] Robotics & 3D Printer Department, Ohsung System Co., Ltd., Ansan 15458, Republic of Korea; jcw4977@ohsungsys.com
[2] Future Bio R&D, EVERIT Co., Ltd., Daejeon 34141, Republic of Korea; archa@everit.kr
[3] Department of Mechatronics Engineering, Hanyang University, Ansan 15588, Republic of Korea
* Correspondence: sdbin225@hanyang.ac.kr

Abstract: Recent advancements in 3D printing technology have integrated with Fourth Industrial Revolution technologies such as robotics and artificial intelligence, aiming to overcome the limitations of conventional manufacturing methods. In the field of functional foods, solvent casting, a common manufacturing technique, has been adopted to produce film-like structures with desired sizes and uniform thickness. However, the typical method of coating or injection on a conventional continuous film is difficult to produce in small amounts. To address this limitation, in the study, we developed a pneumatic pressure syringe-type dispensing system integrated with a food 3D printer utilizing fused deposition modeling (FDM) technology. A syringe type is needed to discharge crude liquid manufactured in the food field in a hygienic environment, and a 3D printing method that is easy to manufacture in small quantities or on demand was utilized. Through simulation and experiment, we wanted to confirm whether stable ejection results are generated according to the selected nozzle-based viscosity, inflow conditions, and the nozzle movement path of the food 3D printer. Based on the nozzle selected through simulation, it was confirmed that the fluid and flow velocity distribution of the viscous material were uniformly distributed and discharged under the conditions of 30,000 cps and inflow rate. By setting the parameters of the food 3D printer and preparing a coenzyme Q10 (CoQ10) sample, we achieved a stable oral dissolving film (ODF) extrusion shape through the design of viscosity and 3D printer nozzle path. The optimal viscosity range for the ODF solution was found to be 25,000 to 35,000 cps, exhibiting precise dimensions and shapes without distortion and yielding the most stable extrusion results. We defined four different nozzle path designs based on minimizing the movement of the 3D printer nozzle. Among them, a 16-step path design demonstrated a stable extrusion method, showing no tailing phenomenon under the conditions of 0.2 MPa pressure and −15.4 KPa vacuum pressure. In future research, we plan to conduct additional research to determine whether the discharge results vary depending on conditions such as viscosity of the crude liquid, nozzle path combination, and ODF thickness.

Keywords: food 3D printer; pneumatic pressure syringe-type dispensing system; oral dissolving films (ODF)

check for updates

Citation: Ji, C.; Cha, A.; Shin, D. Design of Viscosity and Nozzle Path Using Food 3D Printer and Pneumatic Pressure Syringe-Type Dispensing System. *Appl. Sci.* **2023**, *13*, 12234. https://doi.org/10.3390/app132212234

Academic Editor: Paolo Prosposito

Received: 5 October 2023
Revised: 3 November 2023
Accepted: 7 November 2023
Published: 11 November 2023

1. Introduction

Currently, the global society is providing new services with the convergence of technologies that led to the Fourth Industrial Revolution, such as artificial intelligence, 3D printing, and big data. Among these technologies, 3D printing plays a foundational role in various fields, including healthcare, and the automotive and aerospace industries. 3D printing technology has also been applied to processed foods like chocolate, cookies, and pizza, bringing about a transformation in the traditional food processing paradigm by utilizing microwave and air fryer techniques [1–4]. This paradigm shift is extending to the field of functional foods, which is related to health, driven by the influence of the healthcare services industry.

Functional foods are developed with the purpose of absorbing ingredients that cannot be obtained from regular foods, aiming to maintain and enhance health benefits [5]. Recently, products containing ingredients such as red ginseng, collagen, probiotics, coenzyme Q10 (CoQ10), and vitamins have been introduced in film form, departing from traditional pill forms.

Oral dissolving films (ODF) are film-based products that dissolve in the mouth and allow the absorption of ingredients through the oral mucosa [6,7]. The manufacturing processes of ODF products are classified into five categories: solvent casting, semisolid casting, hot melt extrusion, solid dispersion, and rolling, depending on the intended purpose [8,9]. Among these methods, solvent casting is the most widely used. In this process, liquid edible ingredients are coated onto a film substrate, dried, and then transferred in a roll form for cutting into individual slices and packaging [10]. Solvent casting enables the production of film-shaped products with desired sizes and uniform thickness. However, the choice of suitable solvents based on the characteristics of the active pharmaceutical ingredient (API), maintaining the appropriate temperature sensitivity of the API, and maintaining the viscosity of the solution are essential considerations for the polymer used as the film matrix [11]. The general method of coating or injection on a conventional continuous film has a length structure of tens of meters, resulting in a deviation between the first and second half of the equipment, and both the left and right ends of the continuous roll, resulting in about 10∼20% yield loss. There is a problem that it is difficult to produce small amounts, so it is not suitable for various small production systems. Therefore, 3D printing technology was approached to solve these two problems.

3D printers are widely used in the field of personalized and small-scale production, employing various types of extrusion methods [12,13]. The choice of extrusion method depends on the form of materials, such as powder, filament, liquid, or metal, with fused deposition modeling (FDM) being the most common approach. FDM utilizes additive manufacturing (AM) technology, where the material contained in a container or filament maintained at a specific temperature is extruded and cooled as the nozzle moves over the build platform, layer by layer, to create a 3D model [14]. This method can be further classified into inkjet printing, laser-assisted printing, and extrusion-based printing [15–19]. For low-viscosity liquid materials that flow easily, inkjet printing is employed, while extrusion-based printing is used for materials with an appropriate level of viscosity, including liquid or solid materials. In extrusion-based printing, there are classifications based on syringe types such as pneumatic pressure, piston, and screw [20,21]. Laser-assisted printing is preferred for powder materials.

In the food field, hygienic aspects must be considered, so pneumatic methods are mainly used to discharge food ingredients. However, when using this method, the discharged results must be output in a fixed quantity or have a stable shape due to tailing problems. The materials currently used in food 3D printers are still limited, and their application to various foods is limited.

In the study, we utilized an extrusion-based printing method with a pneumatic pressure syringe type in a food 3D printer to extrude CoQ10 with a viscosity similar to chocolate as a material for oral dissolving films (ODF). We compared and validated the performance by setting optimized parameters according to the viscosity and path design of the food 3D printer. The research hypothesis is as follows: The discharge result varies depending on the viscosity of the material and the moving path of the nozzle.

Section 2 introduces the hardware related to the nozzle design of the food 3D printer, that is, a pneumatic pressure syringe-type dispensing system. In the Section 3, experimental pre-settings and procedures are described. Section 4 verifies the research hypothesis through a combination of simulation and experimental environments. Section 5 deals with the conclusion.

2. Hardware Settings

For stable discharge of ODF results, a dedicated nozzle was designed and selected, and a food 3D printer and pneumatic pressure syringe-type dispensing system was manufactured as follows.

2.1. Nozzle Design of Food 3D Printer

ODF is a dried film piece formed by spreading a viscous solution thinly, and to implement it using a food 3D printer, a nozzle for extrusion needs to be fabricated. Considering the viscosity of the feasible solution for ODF, we created dedicated nozzles not only based on the nozzle diameter of conventional food 3D printers but also with different shapes in the supply section. The three types of nozzles used in the experiments are as follows: Nozzle 1 has a medium-sized opening with dimensions of 2.6 mm width and 0.5 mm height. Nozzle 2 has a narrow opening with dimensions of 3 mm width and 0.5 mm height. Nozzle 3 has a wide opening with dimensions of 10 mm width and 1.2 mm height. Dark chocolate was used to extrude the solution in a shape similar to ODF. The default settings of the food 3D printer are as follows: XY-axis resolution of 0.050 mm, $3840 \times 2340(4K)$ resolution, Z axis resolution ranging from 0.01 mm to 0.15 mm, and the output method is material 405 nm UV resin SLA printing. To test the orientation and shape of the nozzle output, the extrusion test was conducted in a linear line within a space of 40 mm width, 17 mm height, and 1 mm depth. The optimal output conditions for each nozzle are as follows: For Nozzle 1, a viscosity of 17,000 cps at 37 °C. For Nozzle 2, a viscosity of 28,000 cps at 35.5 °C. For Nozzle 3, a viscosity of 3000 cps at 39 °C. It was observed that Nozzle 1 exhibited non-uniform extrusion of the solution, and Nozzle 3 experienced dripping of the solution from the nozzle due to a slightly higher preheating temperature, causing the extruder's motor to stop. Thus, it was discovered that even with some variation in viscosity, stable extrusion can be achieved by using an appropriate viscosity solution, activating the reverse extrusion (retraction) function, and creating internal space within the nozzle for stable extrusion. Based on the experimental results, the basic configuration of the nozzle with an internal space was set as Nozzle 2, and to enhance the effectiveness of the operating mechanism, the extrusion outlet was designed as a linear line instead of a point. The solution extruded from the linear outlet can form ODF in a single movement. The final selected nozzle design is shown in Figure 1.

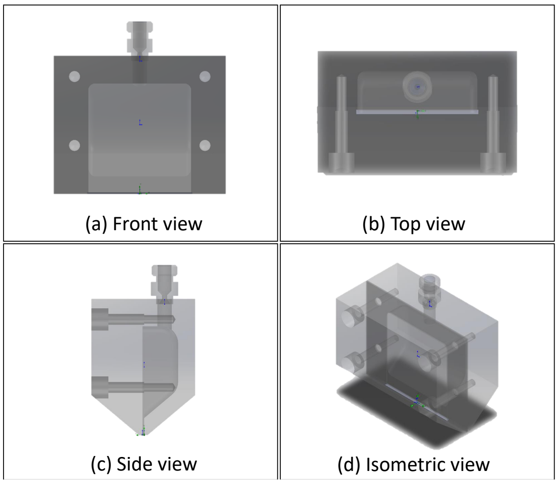

Figure 1. Nozzle geometry: (**a**) front view, (**b**) top view, (**c**) side view, (**d**) isometric view.

2.2. Food 3D Printer and Syringe Dispensing System

The food 3D printer (SMART3D FoodBot, Ohsung Systems) utilizes fused deposition modeling (FDM) as the printing method and consists of a flat nozzle, syringe, syringe holder bracket, and precision leveling bed. The printer has dimensions of $420 \times 381 \times 400$ mm and weighs 15 kg. It supports various materials for printing, including chocolate, mousse, dough, and other viscous substances. The maximum print size is 150 × 150 × 75 mm, and it operates at printing speeds ranging from 15∼70 mm/s. Printing precision is 0.1/100 mm on the XY-axis and 0.01/100 mm on the ZE axis. To enable ODF extrusion, the food 3D printer was modified into a pneumatic extrusion system, and a dispenser was created. The dispenser includes separate components for vacuum generation and extrusion pressure generation, each equipped with pressure sensors to monitor the set and current pressures in real time. The vacuum pressure range is −100∼0 KPa, while the extrusion pressure range is 0∼0.9 MPa. The pressure control unit is implemented using a linear circuit, and the switch is an analog dial. The sensitivity can be adjusted with intervals of 0.01 KPa for vacuum pressure and within a range of 0.01 MPa for extrusion pressure. The syringe dispensing system, as shown in Figure 2, is equipped with a pneumatic control module. Through this device, the air pressure is regulated to deliver pneumatic pressure to the syringe, which is fixed in the bracket inside the food 3D printer, resulting in the extrusion of the material contained within the syringe.

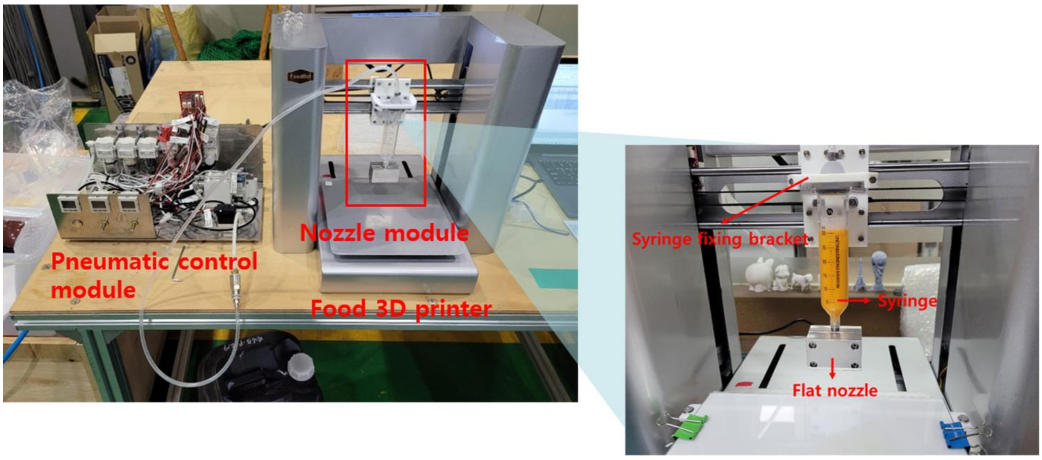

Figure 2. Hardware for food 3D printer and syringe dispensing system.

2.3. Pneumatic Control Module

The overall operating sequence of the pneumatic control module is shown in Figure 3. Initially, the air passes through a three-stage filtration system consisting of an air filter, dust filter 1, and dust filter 2. The air filter removes impurities from the air drawn into the pressure generation unit, while dust filter 1 and dust filter 2 control the particle size of airborne dust particles to 0.3 µm and 0.01 µm, respectively. The filtered air is then drawn in through the pressure relief 3-port valve, and the pressure within the system is regulated to fall within the range of 0.3∼0.5 MPa using a pressure sensor. The supplied air is utilized for vacuum generation and supply pressure control. The vacuum generation process is as follows. To provide consistent pressure from irregular air pressure, the pressure of the pneumatic regulator (ARM10 series, SMC) is manually set to 0.35 MPa, and the pressure generator, i.e., the ejector (ZK2 series, SMC), creates a vacuum state. The electro-pneumatic regulator (EPR) adjusts the pressure for the vacuum within the range of −100∼0 KPa, generating precise vacuum pressure. A pressure sensor senses the accuracy of the vacuum pressure, and it is then connected to the 3-port solenoid valve 3 to switch the vacuum state for use. The supply pressure control process is separate from the vacuum generation process. The supplied air pressure is regulated within the range of 0∼0.9 MPa using the EPR device. A pressure sensor senses the numerical value of the pressure, and it is connected to the 3-port solenoid valve 1, increasing the internal air pressure. Finally, the 3-port solenoid valve 2 is connected to the syringe. The operating principle of the 3-port solenoid valve is as follows. When the control switch attached to the syringe dispensing system is activated, it increases the internal air pressure within the syringe through the path from 1 to 2, causing the ejection of the liquid contained in the syringe. When the control switch is not activated, the supplied air is blocked, and the air is exhausted from 2 to 3. At this time, the internal state of the syringe becomes a vacuum, causing the cessation of liquid discharge.

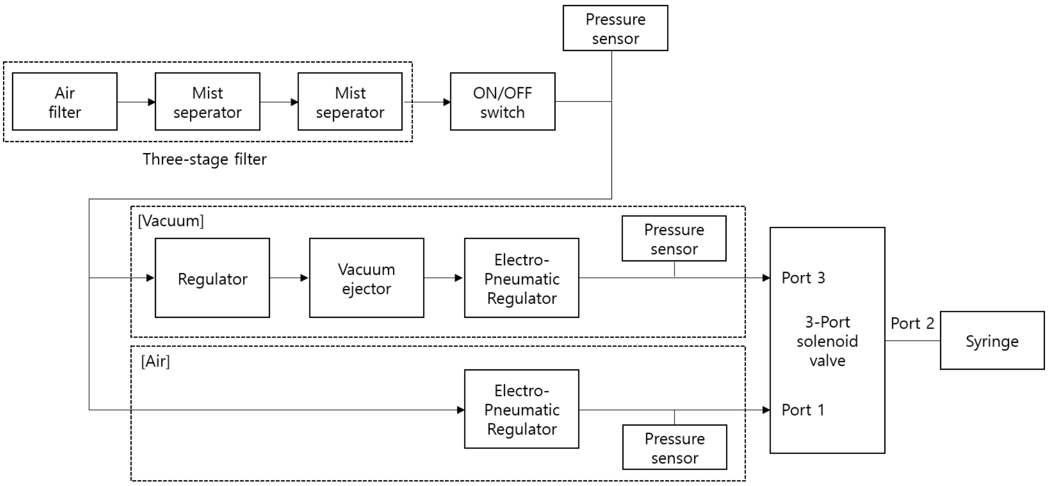

Figure 3. The operating sequence of the pneumatic control module.

3. Methodology

3.1. Experiment Pre-Settings

3.1.1. Parameter Settings of Food 3D Printer

For the ODF output from the food 3D printer to have commercial value, the printing process needs to be standardized. Specific parameter values for controlling the shape formation were defined based on the input values of the food 3D printer, as shown in Table 1. The parameters for controlling the movement of the nozzle were specified as constants and variables. Offset, output position, and extrusion-related parameters determine the movement of the nozzle. To standardize the movement of the nozzle, these parameters were set as constants. The offset parameter represents the additional height parameter H_1 during nozzle movement and the glass bed device H_2 offset amount. This value influences the gap between the nozzle and the bed, and an incorrect value can result in distorted or misaligned output shapes. The optimal values for (H_1, H_2) were determined as (10, 28). The output position parameters, P_x for the X-coordinate and P_y for the Y-coordinate at the center of the output were set to (100, 100), representing the point where the output material falls on the bed with the highest horizontal stability. The extrusion-related parameters control the stable discharge of the liquid from the nozzle. The extruded amount is controlled by the air pressure E_s, the retraction size represents the vacuum pressure magnitude E_r, and the pre-output E-position E_1 and post-output E-position E_2 are parameters that help reduce output errors at the start and end points of the output. To minimize tailing at the endpoint, when using a viscosity of 30,000 cps, (E_1, E_2) were set to (0.00017, 0.032). The variables to be manipulated are the output thickness T_w, output speed V, and output length W. T_w influences the actual height of the output. V represents the nozzle's speed when the material is extruded and needs to be matched precisely with the extrusion speed E_s to produce optimal output. Finally, W represents the length of the trajectory of the flat-type nozzle's movement.

Table 1. Parameter settings of food 3D printer.

No.	Parameter	Variable	Explanation	Value
1	Offset	H_1	Extra height when moving the nozzle	10
2		H_2	Offset of glass bed device	28
3	Thickness	T_w	Output thickness	0.5
4	Speed	V	Output speed (mm/s)	15
5	Length	W	Output length	30
6	Location	P_x	Center X position of printout	100
7		P_y	Center Y position of printout	100
8	Extrusion	E_s	E-steps per unit	1067
9		E_r	Retraction size	−2
10		E_1	Ready for output E position	0.00017
11		E_2	E position after output	0.032

3.1.2. CoQ10 Manufacturing

In order to be discharged in the form of ODF, a food material, a uniform size and a fixed amount of CoQ10 crude solution are required. Food 3D printing technology is suited to these characteristics. Coenzyme Q10 (CoQ10), which accounts for the largest amount among Vitamin A, CoQ10, and lycopene, was selected as the undiluted solution used in the experiment. The undiluted solution was received from EVERIT. For each ODF unit, various additives were incorporated in descending order of their concentration ratios, as shown in Table 2. The additives included CoQ10, HPMC, β-Cyclodextrin, pectin, and glycerin. A total of seven different samples were prepared by adding 10g each of purified water.

Table 2. CoQ10 manufacturing ingredients.

Material Name	Material Information	Based on 1 Sheet of ODF	
		Amount (mg)	Ratio (%)
CoQ10	Functional 90∼100 mg	100.00	31.77
HPMC	AN6	60.00	19.06
HPMC	AN15	60.00	19.06
β-cyclodextrin	Solubilizing agent	50.00	15.88
Pectin	Give strength	15.00	4.76
Glycerin	Plasticizer	12.00	3.81
Propylene glycol	Less than 2% (Before adding food)	5.50	1.75
Arginine	Solubilizing agent	5.00	1.59
Pomegranate scent	Flavoring agent	5.00	1.59
Polysorbate 80	Surfactants twin80	1.00	0.32
Polysorbate 20	Surfactants twin20	1.00	0.32
Sucralose	Sweetener	0.30	0.10
Purified water	-	300.00	-
Sum of solids (mg)		314.80	100.00

3.2. *Experimental Procedure*

Through a combination of simulation and experimental environments, the goal is to examine material ejection trends according to material viscosity conditions and path settings of a food 3D printer.

3.2.1. Simulation Environment

Based on the selected nozzle, we check whether the discharge result varies depending on the viscosity. The material used is chocolate as a substitute for ODF. The material has viscosity, and discharge is affected by the internal shape and volume of the nozzle [22–24]. The analysis will be conducted on three viscosity conditions: low viscosity, high viscosity, and high viscosity and mass inflow. The conditions for low viscosity are as follows: At a temperature of 20 °C, atmospheric pressure, and an inflow rate of 0.1 kg/s, water exhibits a viscosity of 1 cps, which is considered low viscosity. The conditions for high viscosity are as follows: It is set to 30,000 cps, which is the maximum value that can be set in ODF. The conditions for high viscosity and mass inflow are as follows: It is assumed that if the high viscosity of 30,000 cps increases by five times the inflow volume, the inlet pressure also increases by five times.

3.2.2. Test Environment

We check whether the ODF results would vary depending on the viscosity of the material and the nozzle path of the 3D printer. The viscosity conditions of the material are set to low viscosity (25,000∼35,000 cps), medium viscosity (40,000∼100,000 cps), and high viscosity (100,000∼200,000 cps) based on 30,000 cps. Four nozzle paths for food 3D printers are selected based on optimal viscosity. For the first condition, a 14-step motion path consisting of 23 codes is designed to minimize nozzle movement (see Appendix A). In the second condition, a 14-step motion path consisting of 24 codes is implemented, aiming to address the trailing issue identified in the first condition through cutting operations (see Appendix B). In the third condition, a 15-step motion path with 25 codes is set, incorporating additional XY-axis movements to correct trailing effects (see Appendix C). In the last condition, a 16-step motion path consisting of 25 codes is implemented (see Appendix D). The size of the extruded ODF material is set to 30×30 mm^2 for the output.

4. Results and Discussion

4.1. Flow Analysis of Viscosity Conditions in Simulation

The results of the analysis divided into three conditions are shown in Figure 4.

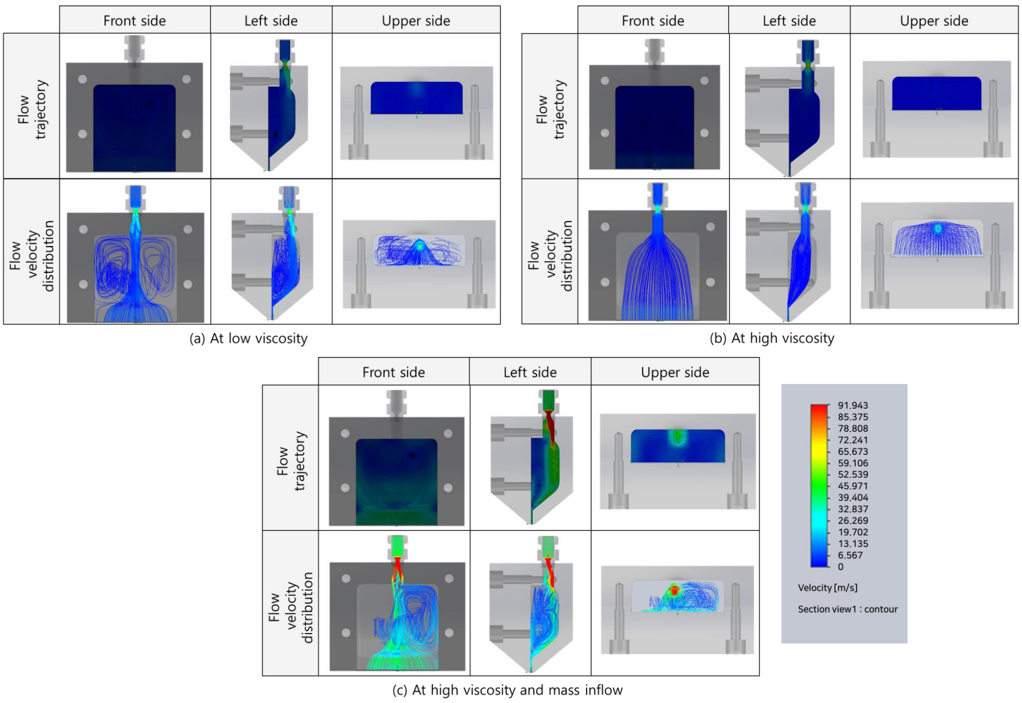

Figure 4. Flow trajectory and velocity distribution according to viscosity conditions.

4.1.1. Low Viscosity Condition

When the fluid fills the slot except for the neck section, the flow velocity remains nearly constant at 13 m/s, but the flow distribution is asymmetric, with vortices formed in various locations in the lower region. The rotational vortices occurring within the slot hinder the consistent extrusion of the fluid. In the flow trajectory, the particle flow within the slot deviates asymmetrically towards one side, and significant vortices occur at the neck section and three locations inside the slot. Such vortex phenomena occurred with a mass inflow in the slot, hindering the consistent extrusion of the fluid. In the flow trajectory, the particle flow within the slot deviates asymmetrically towards one side, and significant vortices occur at the neck section and three locations inside the slot. Such vortex phenomena occurred with a mass inflow of 0.1 kg/s and up to a maximum viscosity of 15,000 cps.

4.1.2. High Viscosity Condition

When the slot is filled with fluid, the flow viscosity remains constant below 13 m/s, and no rotational vortices occur within the slot. In the flow trajectory, the fluid spreads evenly from the center to the left and right, enabling a consistent extrusion. This phenomenon indicates that the slot's internal space temporarily stores the fluid and allows for stable and controlled output during extrusion. With a mass inflow of 0.1 kg/s and a maximum viscosity ranging from 20,000 to 35,000 cps, stable extrusion is achievable.

4.1.3. High Viscosity and Mass Inflow Conditions

With the increased mass inflow, similar to the low viscosity case, asymmetrical vortices occur in the front, back, left, and right directions. This phenomenon indicates a correlation between viscosity and extrusion volume, where lower viscosity and higher mass inflow result in a higher likelihood of vortices. For a viscosity of 30,000 cps, stable extrusion is achievable for a mass inflow ranging from 0.078 to 0.247 kg/s.

4.2. ODF Results according to Viscosity Conditions

Based on the previously set 3D printer parameter conditions, the results of the ODF extrusion were analyzed according to the viscosity ranges of the sample solution. The evaluation criteria for the results were whether the discharge shape was distorted or tailing occurred. The ODF results are shown in Table 3. For high viscosity (100,000∼200,000 cps), the high flow rate inside the nozzle leads to internal backflow phenomena. Additionally, empty spaces are formed within the nozzle, resulting in inconsistent extrusion speed. While one side of the nozzle exhibited smooth output, the shape on the other side was distorted. For medium viscosity (40,000∼100,000 cps), the excessive solution was extruded, leading to overall distortion of the shape. At the optimal viscosity range (25,000∼35,000 cps), which showed the most stable output in the simulation tests, precise dimensions and shapes were observed during extrusion. However, due to the omission of the retraction function and path optimization process, there were extrusion errors at the starting point and trailing effects at the endpoint.

Table 3. ODF results according to viscosity conditions.

Discharge Direction	Range of Centipose(cps)		
	25,000∼35,000	40,000∼100,000	100,000∼200,000
Width	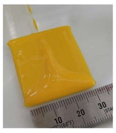		
Length			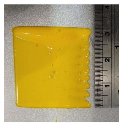

4.3. ODF Results according to Path Design of Food 3D Printer

Using the optimal viscosity of the prepared solution, ODF shapes were compared and analyzed based on different motion path settings of the 3D printer. The evaluation criteria for the results were whether it was output in a uniform size, whether tailing occurred, and whether the discharge shape was uniform. The ODF results according to the path design of the food 3D printer are shown in Table 4. In the first condition, the output quality was the most favorable when the extrusion pressure was set to 0.15 MPa and the vacuum pressure was set to −10.4 KPa. The size of the output fell within the range of 31×31 mm^2, with an acceptable deviation from the target size of 30×30 mm^2. However, trailing effects were observed at the end, resulting in non-uniform thickness. In the second condition, the optimal output state was achieved with an extrusion pressure of 0.18 MPa and a vacuum pressure of −7.2 KPa. The output size measured 33×32 mm^2, which is slightly larger due to the inclusion of cutting codes, although the actual cutting effect was not evident. However, the thickness of the output was not uniform, as it became too thin and deformed after drying. In the third condition, the added path involved a 20-unit movement along the Y-axis and a cutting command by narrowing the gap between the bed and the nozzle. The optimal output state was achieved with an extrusion pressure of 0.21 MPa and a vacuum pressure of −8.4 KPa, resulting in an output size of 32×31 mm^2. While the thickness of the extruded solution was uniform, the ODF exhibited difficulty in detaching from the bed after drying. In the last condition, an additional −0.05 Z-axis movement was included to address trailing effects. The optimal output state was achieved with an extrusion pressure of 0.2 MPa and a vacuum pressure of −15.4 KPa, resulting in an output size of 31×32 mm^2 without any trailing effects.

Table 4. ODF results according to path design of food 3D printer.

Discharge Direction	Path Design			
	1st Condition	2nd Condition	3rd Condition	4th Condition
Width		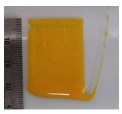	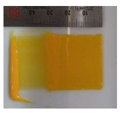	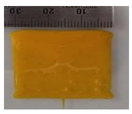
Length	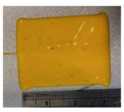	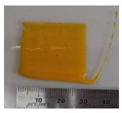	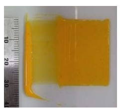	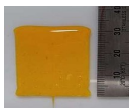

5. Conclusions

We developed a pneumatic pressure syringe-type dispensing system integrated with a food 3D printer. Through simulations, we determined the optimal viscosity coefficient and hydraulic conditions by analyzing the flow rate and distribution of a viscous solution to achieve a stable and controlled extrusion of the solution. CoQ10 was used as a sample solution for testing, and we compared and analyzed the extrusion results of ODF based on the viscosity of the solution and the motion path settings of the food 3D printer. The optimal viscosity range for the ODF solution was found to be 25,000∼35,000 cps, which demonstrated accurate dimensions and shapes without distortion, resulting in the most stable extrusion. We designed four different motion path settings for the food 3D printer's nozzle, focusing on minimizing nozzle movement. Among them, the dispensing method using a 16-step motion path exhibited stability, and when the extrusion pressure was set to 0.2 MPa and the vacuum pressure to −15.4 KPa, no trailing effects were observed. It was confirmed that the result of the discharge shape varies depending on the research hypothesis, viscosity of the crude liquid and nozzle path settings, and stable discharge was confirmed through the absence of the tailing phenomenon and uniform size measurement. In the future, we plan to conduct additional research to determine whether the discharge results vary depending on conditions such as viscosity of the crude liquid, nozzle path combination, and ODF thickness.

Author Contributions: Conceptualization, C.J. and D.S.; methodology, C.J.; software, C.J.; validation, C.J. and D.S.; formal analysis, C.J.; investigation, C.J.; resources, C.J. and A.C.; data curation, D.S.; writing—original draft preparation, C.J.; writing—review and editing, D.S.; visualization, C.J.; supervision, D.S.; project administration, D.S.; funding acquisition, C.J. All authors have read and agreed to the published version of the manuscript.

Funding: This work was supported by the Korea Institute of Planning and Evaluation for Technology in Food, Agriculture and Forestry(IPET) through High Value-added Food Technology Development Program, funded by Ministry of Agriculture, Food and Rural Affairs(MAFRA)(121018-3).

Institutional Review Board Statement: Not applicable.

Informed Consent Statement: Not applicable.

Data Availability Statement: Data is contained within the article.

Conflicts of Interest: Author Changuk Ji was employed by the company Robotics & 3D Printer Department, Ohsung System Co., Ltd. The remaining authors declare that the research was conducted in the absence of any commercial or financial relationships that could be construed as a potential conflict of interest. Author Areum Cha was employed by the company Future Bio R&D, EVERIT Co., Ltd. The remaining authors declare that the research was conducted in the absence of any commercial or financial relationships that could be construed as a potential conflict of interest.

Abbreviations

The following abbreviations are used in this manuscript:

UV	Ultraviolet
SLA	Stereolithography

Appendix A

Table A1. Moving path test for 1st condition.

Path	No.	G-Code	Variable	Command	Explanation
1	1 2 3 4	M92 E1067 G21 G90 M82	E_s	"M92 E", E_s	Ready to start printing (No movement)
2	5	G28 X0 Y0			XY-axis home position
3	6	G28 Z0			Z-axis home position
4	7	G1 Z38 F3000	H_1, H_2	"G1 Z", (H_1 + H_2), "F3000"	Z-axis movement (Ready for output)
5	8	G1 F9000 X100	P_x	"G1 F9000 X", P_x	X-axis movement (Ready for output)
6	9 10 11 12	G92 E0 G1 F300 E4.5 G92 E0 G1 F3000 E-2	E_r	"G1 F3000 E", E_r	Ready for extruder output (No movement)
7	13	G1 Y115	P_y, W	"G1 Y", $(P_y + W/2)$	Move to Y-axis output position
8	14	G0 F4800 Z28.5	T_w, H_2	"G0 F4800 Z", $(T_w + H_2)$	Z-axis movement (Print thickness position)
9	15 16	G1 F3000 E0.0 G1 F900 E0.00017	V, E_1	"G1 F", $(V * 60)$, "E", E1	Prepare the extruder (No movement)
10	17	G1 Y85 E0.032	P_y, W, E_2	"G1 Y", $(P_y - W/2)$, "E", E_2	Discharge movement as much as Y-axis output length
11	18	G1 F3000 E-1.968	E_2, E_r	"G1 F3000 E", $(E_2 - E_r)$	Extruder retreat (No movement)
12	19	G0 F4800 Z38	H_1, H_2	G0 F4800 Z", $(H_1 + H_2)$	Z-axis movement upward as much as Z+10 after dispensing is completed
13	20	G28 Y0			Y-axis home position
14	21 22 23	G91 G1 E-3 F300 M84 G90			Exit after completion of output (No movement)

Appendix B

Table A2. Moving path test for 1st condition.

Path	No.	G-Code	Variable	Command	Explanation
1	1 2 3 4	M92 E1067 G21 G90 M82	E_s	"M92 E",E_s	Ready to start printing (No movement)
2	5	G28 X0 Y0			XY-axis home position
3	6	G28 Z0			Z-axis home position
4	7	G1 Z38 F3000	H_1, H_2	"G1 Z", $(H_1 + H_2)$, "F3000"	Z-axis movement (Ready for output)
5	8	G1 F9000 X100	P_x	"G1 F9000 X", P_x	X-axis movement (Ready for output)
6	9 10 11 12	G92 E0 G1 F300 E4.5 G92 E0 G1 F3000 E-2	E_r	"G1 F3000 E", E_r	Ready for extruder output (No movement)
7	13	G1 Y115	P_y, W	"G1 Y",$(P_y + W/2)$	Move to Y-axis output position
8	14	G0 F4800 Z28.5	T_w, H_2	"G0 F4800 Z", $(T_w + H_2)$	Z-axis movement (Print thickness position)
9	15 16	G1 F3000 E0.0 G1 F900 E0.00017	V, E_1	"G1 F", $(V * 60)$, "E", E_1	Prepare the extruder (No movement)
10	17	G1 Y85 E0.032	P_y, W, E_2	"G1 Y", $(P_y - W/2)$, "E", E_2	Discharge movement as much as Y-axis output length
11	18	G1 F3000 E-1.968	E_2, E_r	"G1 F3000 E", $(E_2 - E_r)$	Extruder retreat (No movement)
12	19	G0 F14400 Y75 Z38	H_1, H_2, P_y, W	G0 F14400 Y", $(P_y - W/2) - 10$, "Z", $(H_1 + H_2)$	Z-axis movement, Y+10, Z+10, move up after dispensing is completed
13	20	G0 F4800 X140	P_x, W	"G0 F4800 X", $P_x + W + 10$	X-axis output avoidance movement
14	21	G28 Y0			Y-axis home position
15	22 23 24	G91 G1 E-3 F300 M84 G90			Exit after completion of output (No movement)

Appendix C

Table A3. Moving path test for 1st condition.

Path	No.	G-Code	Variable	Command	Explanation
1	1 2 3 4	M92 E1067 G21 G90 M82	E_s	"M92 E", E_s	Ready to start printing (No movement)
2	5	G28 X0 Y0			XY-axis home position
3	6	G28 Z0			Z-axis home position
4	7	G1 Z38 F3000	H_1, H_2	"G1 Z", $(H_1 + H_2)$, "F3000"	Z-axis movement (Ready for output)
5	8	G1 F9000 X100	P_x	"G1 F9000 X", P_x	X-axis movement (Ready for output)
6	9 10 11 12	G92 E0 G1 F300 E4.5 G92 E0 G1 F3000 E-2	E_r	"G1 F3000 E", E_r	Ready for extruder output (No movement)
7	13	G1 Y115	P_y, W	"G1 Y", $(P_y + W/2)$	Move to Y-axis output position
8	14	G0 F4800 Z28.5	T_w, H_2	"G0 F4800 Z", $(T_w + H_2)$	Z-axis movement (Print thickness position)
9	15 16	G1 F3000 E0.0 G1 F900 E0.00017	V, E_1	"G1 F", $(V * 60)$, "E", E_1	Prepare the extruder (No movement)
10	17	G1 Y85 E0.032	P_y, W, E_2	"G1 Y", $(P_y - W/2)$, "E", E_2	Discharge movement as much as Y-axis output length
11	18	G1 F3000 E-1.968	E_2, E_r	"G1 F3000 E", $(E_2 - E_r)$	Extruder retreat (No movement)
12	19	G1 Z28	H_2	"G1 Z", H_2	Z-axis movement and nozzle, base plate spacing 0
13	20	G0 F4800 Y65	P_y, W	"G0 F4800 Y", $(P_y - W/2) - 20$	Move Y-axis by 20
14	21	G0 X140 Z38	P_x, W, H_1, H_2	"G0 X", $P_x + W + 10$, "Z", $(H_1 + H_2)$	Avoid XZ-axis simultaneous movement output
15	22	G28 Y0			Y-axis home position
16	23 24 25	G91 G1 E-3 F300 M84 G90			Exit after completion of output (No movement)

Appendix D

Table A4. Moving path test for 1st condition.

Path	No.	G-Code	Variable	Command	Explanation
1	1 2 3 4	M92 E1067 G21 G90 M82	E_s	"M92 E",E_s	Ready to start printing (No movement)
2	5	G28 X0 Y0			XY-axis home position
3	6	G28 Z0			Z-axis home position
4	7	G1 Z38 F3000	H_1, H_2	"G1 Z", $(H_1 + H_2)$, "F3000"	Z-axis movement (Ready for output)
5	8	G1 F9000 X100	P_x	"G1 F9000 X", P_x	X-axis movement (Ready for output)
6	9 10 11 12	G92 E0 G1 F300 E4.5 G92 E0 G1 F3000 E-2	E_r	"G1 F3000 E", E_r	Ready for extruder output (No movement)
7	13	G1 Y115	P_y, W	"G1 Y", $(P_y + W/2)$	Move to Y-axis output position
8	14	G0 F4800 Z28.5	T_w, H_2	"G0 F4800 Z", $(T_w + H_2)$	Z-axis movement (Print thickness position)
9	15 16	G1 F3000 E0.0 G1 F900 E0.00017	V, E_1	"G1 F", $(V * 60)$, "E", E_1	Prepare the extruder (No movement)
10	17	G1 Y85 E0.032	P_y, W, E_2	"G1 Y", $(P_y - W/2)$, "E", E_2	Discharge movement as much as Y-axis output length
11	18	G1 F3000 E-1.968	E_2, E_r	"G1 F3000 E", $(E_2 - E_r)$	Extruder retreat (No movement)
12	19	G1 F9000 Z27.95	H_1, H_2	"G1 Z", $(H_1 - H_2)$	Tuning work with Z-axis movement and nozzle, bottom plate spacing −0.05
13	20	G0 F4800 Y65	P_y, W	"G0 F4800 Y", $(P_y - W/2) - 20$	Move Y-axis by 20
14	21	G0 X140 Z38	P_x, W, H_1, H_2	"G0 X", $P_x + W + 10$, "Z", $(H_1 + H_2)$	Avoid XZ-axis simultaneous movement output
15	22	G28 Y0			Y-axis home position
16	23 24 25	G91 G1 E-3 F300 M84 G90			Exit after completion of output (No movement)

References

1. Pallottino, F.; Hakola, L.; Costa, C.; Antonucci, F.; Figorilli, S.; Seisto, A.; Menesatti, P. Printing on food or food printing: A review. *Food Bioprocess Technol.* **2016**, *9*, 725–733. [CrossRef]
2. Yang, F.; Zhang, M.; Bhandari, B. Recent development in 3D food printing. *Crit. Rev. Food Sci. Nutr.* **2017**, *57*, 3145–3153. [CrossRef] [PubMed]
3. Dankar, I.; Haddarah, A.; Omar, F.E.; Sepulcre, F.; Pujolà, M. 3D printing technology: The new era for food customization and elaboration. *Trends Food Sci. Technol.* **2018**, *75*, 231–242. [CrossRef]
4. In, J.; Jeong, H.; Min, S.C. Material requirements for printing cookie dough using a fused deposition modeling 3D printer. *Food Sci. Biotechnol.* **2022**, *31*, 807–817. [CrossRef]
5. Martirosyan, D.M.; Singh, J. A new definition of functional food by FFC: What makes a new definition unique? *Funct. Foods Health Dis.* **2015**, *5*, 209–223. [CrossRef]

6. Salawi, A. An insight into preparatory methods and characterization of orodispersible film—A review. *Pharmaceuticals* **2022**, *15*, 844. [CrossRef] [PubMed]
7. Hoffmann, E.M.; Breitenbach, A.; Breitkreutz, J. Advances in orodispersible films for drug delivery. *Expert Opin. Drug Deliv.* **2011**, *8*, 299–316. [CrossRef]
8. Lee, G.W.; Jeong, H. Development and evaluation of orodispersible films for oro-mucosal application. *Rev. Korea Contents Assoc.* **2016**, *14*, 47–54.
9. Dong, J.; Li, Y.; Lin, P.; Leeflang, M.; Van Asperen, S.; Yu, K.; Tümer, N.; Norder, B.; Zadpoor, A.; Zhou, J. Solvent-cast 3D printing of magnesium scaffolds. *Acta Biomater.* **2020**, *114*, 497–514. [CrossRef]
10. Juluru, N.S. Fast dissolving oral films: A review. *IJAPBC* **2013**, *2*, 108–112.
11. Mishra, R.; Amin, A. Manufacturing techniques of orally dissolving films. *Pharm. Technol.* **2011**, *35*, 70–73.
12. Liu, Y.; Liang, X.; Saeed, A.; Lan, W.; Qin, W. Properties of 3D printed dough and optimization of printing parameters. *Innov. Food Sci. Emerg. Technol.* **2019**, *54*, 9–18. [CrossRef]
13. Vancauwenberghe, V.; Verboven, P.; Lammertyn, J.; Nicolaï, B. Development of a coaxial extrusion deposition for 3D printing of customizable pectin-based food simulant. *J. Food Eng.* **2018**, *225*, 42–52. [CrossRef]
14. Tan, C.; Toh, W.Y.; Wong, G.; Li, L. Extrusion-based 3D food printing—Materials and machines. *Int. J. Bioprint.* **2018**, *4*, 143. [CrossRef] [PubMed]
15. Godoi, F.C.; Prakash, S.; Bhandari, B.R. 3d printing technologies applied for food design: Status and prospects. *J. Food Eng.* **2016**, *179*, 44–54. [CrossRef]
16. Chen, D.X. Extrusion bioprinting of scaffolds. In *Extrusion Bioprinting of Scaffolds for Tissue Engineering Applications*; Springer: Cham, Switzerland, 2019; pp. 117–145.
17. Liu, Z.; Zhang, M.; Bhandari, B.; Wang, Y. 3D printing: Printing precision and application in food sector. *Trends Food Sci. Technol.* **2017**, *69*, 83–94. [CrossRef]
18. Sun, J.; Peng, Z.; Zhou, W.; Fuh, J.Y.; Hong, G.S.; Chiu, A. A review on 3D printing for customized food fabrication. *Procedia Manuf.* **2015**, *1*, 308–319. [CrossRef]
19. Portanguen, S.; Tournayre, P.; Sicard, J.; Astruc, T.; Mirade, P.S. Toward the design of functional foods and biobased products by 3D printing: A review. *Trends Food Sci. Technol.* **2019**, *86*, 188–198. [CrossRef]
20. Kewuyemi, Y.O.; Kesa, H.; Adebo, O.A. Trends in functional food development with three-dimensional (3D) food printing technology: Prospects for value-added traditionally processed food products. *Crit. Rev. Food Sci. Nutr.* **2021**, *62*, 7866–7904. [CrossRef]
21. Jeong, H.J.; Nam, H.; Jang, J.; Lee, S.J. 3D bioprinting strategies for the regeneration of functional tubular tissues and organs. *Bioengineering* **2020**, *7*, 32. [CrossRef]
22. Guo, C.; Zhang, M.; Bhandari, B. Model building and slicing in food 3D printing processes: A review. *Compr. Rev. Food Sci. Food Saf.* **2019**, *18*, 1052–1069. [CrossRef] [PubMed]
23. Lanaro, M.; Forrestal, D.P.; Scheurer, S.; Slinger, D.J.; Liao, S.; Powell, S.K.; Woodruff, M.A. 3D printing complex chocolate objects: Platform design, optimization and evaluation. *J. Food Eng.* **2017**, *215*, 13–22. [CrossRef]
24. Karyappa, R.; Hashimoto, M. Chocolate-based ink three-dimensional printing (Ci3DP). *Sci. Rep.* **2019**, *9*, 14178. [CrossRef] [PubMed]